RSC Advances

PAPER

View Article Online
View Journal | View Issue

Cite this: *RSC Adv.*, 2023, **13**, 35583

Synthesis and evaluation of tirbanibulin derivatives: a detailed exploration of the structure–activity relationship for anticancer activity†

Jaebeom Park,[ab] Minji Kang,[ac] Ahyoung Lim,[a] Kyung-Jin Cho,[a] Chong Hak Chae,[a] Byumseok Koh *[ac] and Hongjun Jeon *[ac]

Tirbanibulin, an FDA-approved microtubule-targeting agent (MTA) introduced in 2020, represents a pioneering treatment for precancerous actinic keratosis. Despite its failure to gain approval as an anticancer agent due to insufficient efficacy, there remains potential value in extending its application into malignancy treatment through tirbanibulin-based derivatives. Tirbanibulin possesses a distinctive dual mechanism of action involving microtubule and Src inhibition, distinguishing it from other MTAs. In spite of its unique profile, exploration of tirbanibulin's structure–activity relationship (SAR) and the development of its derivatives are significantly limited in the current literature. This study addresses this gap by synthesizing various tirbanibulin derivatives and exploring their SAR through modifications in the core amide motif and the eastern benzylamine part. Our results underscore the critical role of the pyridinyl acetamide core structure for optimal cellular potency, with favorable tolerance observed for modifications at the *para* position of the benzylamine moiety. Particularly noteworthy is the analogue modified with *p*-fluorine benzylamine, which exhibited favorable *in vivo* PK profiles. These findings provide crucial insights into the potential advancement of tirbanibulin-based compounds as promising anticancer agents.

Received 6th October 2023
Accepted 30th November 2023

DOI: 10.1039/d3ra06790d

rsc.li/rsc-advances

Introduction

Since cell cycle dysregulation is a hallmark of cancer, and targeting mitosis remains a mainstay of anticancer therapy.[1–5] The most representative drugs in this category are microtubule-targeting agents (MTAs). MTAs disrupt microtubule dynamics by stabilizing or destabilizing microtubules, leading to cell cycle arrest at the G2/M phase and, ultimately apoptosis.[6–9] Paclitaxel (**1**, Chart 1) and ixabepilone (**2**) are microtubule-stabilizing agents. Vinca alkaloids, exemplified by **3** and **4**, as well as eribulin (**5**), function as microtubule-destabilizing agents. Other mitosis-targeted drugs have been developed, such as aurora kinase,[10] polo-like kinase-1,[11] and motor protein inhibitors.[12,13] However, owing to their limited efficacy as anticancer agents, these drugs have not yet been approved by the FDA, suggesting the effectiveness of direct targeting of microtubules. Indeed, microtubules play a critical

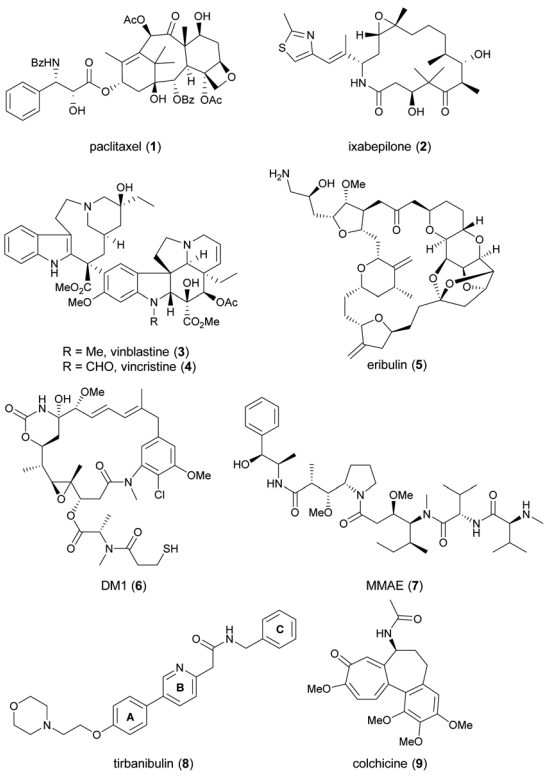

Chart 1 The structures of microtubule-targeting agents.

[a]*Therapeutics & Biotechnology Division, Korea Research Institute of Chemical Technology, Daejeon 34114, Republic of Korea. E-mail: bkoh@krict.re.kr; hjeon@krict.re.kr*

[b]*College of Pharmacy, Chungbuk National University, Cheongju 28160, Republic of Korea*

[c]*Medicinal Chemistry & Pharmacology, University of Science & Technology, Daejeon 34113, Republic of Korea*

† Electronic supplementary information (ESI) available. See DOI: https://doi.org/10.1039/d3ra06790d

role throughout the cell cycle, and are involved in mitosis-independent cellular functions such as intracellular trafficking, angiogenesis, and metastasis-related cell migration.[5,14] Recently, MTAs have regained attention, as evidenced by the incorporation of chemically modified synthetic drugs like DM1 (**6**) and MMAE (**7**) into antibody–drug conjugates (ADCs), a promising modality for cancer treatment.[15]

An emerging approach in the development of new MTAs, aiming for enhanced clinical efficacy and reduced undesired effects, is the design of dual-target inhibitors with synergistic effects.[16,17] Active efforts have been made to modify MTAs to confer an additional inhibitory ability on kinases, histone deacetylases, estrogen receptor, or immune-related targets.[16] The sole successful MTA in this class is tirbanibulin (**8**, KX-01, Chart 1), which received approval from the U.S. Food and Drug Administration in 2020 under the trade name Klisyri®.

Tirbanibulin possesses dual mechanism of action (MOA), combining Src signaling inhibition and disruption of microtubule dynamics,[18–20] the latter of which was identified during a phase 2 trial.[20] Initially developed as an anticancer drug for patients with bone metastatic castration-resistant prostate cancer who had not received prior chemotherapy, tirbanibulin failed to meet the efficacy endpoint in a phase 2 trial (NCT01074138).[21] It was later repurposed for dermatological use, in the form of an ointment (NCT03285477 and NCT03285490), and approved by the FDA as a first-in-class medication for the treatment of pre-cancerous actinic keratosis on the face or scalp.[22] Recently, indication expansion studies for tirbanibulin are under investigation for basal cell carcinoma (NCT05713760 and NCT06112522)[23] and plaque-type psoriasis (NCT05522816).[24]

Tirbanibulin exhibits distinctive features. It shows significant *in vitro* antitumor activity with nanomolar IC_{50} values, even against tumor cell lines that have developed resistance to dasatinib, a multi-kinase inhibitor targeting Src, owing to its dual MOA.[18–20] Furthermore, tirbanibulin has demonstrated low toxicity in preclinical and clinical studies, attributed to its reversible binding to the colchicine (**9**)-binding site of β-tubulin.[25]

Despite its unique antitumor MOA and low clinical toxicity, there has been limited effort towards synthesizing tirbanibulin-based derivatives or elucidating the associated structure–activity relationship (SAR). To the best of our knowledge, only two medicinal chemistry studies on tirbanibulin's structure have been reported in journals.[26,27] The research reported in 2011 replaced the pyridine ring (B-ring) of tirbanibulin with thiazole, resulting in thiazolyl derivatives with only micromolar GI_{50} values.[26] The recent study published in 2021 focused on altering the western morpholine part to enhance its antiproliferative effect.[27] However, other segments of tirbanibulin, like the core amide motif and the A- or C-rings, remain unexplored. In this study, we examined structural variations in the core amide motif and the eastern benzylamine portion (C-ring) while evaluating the antitumor effects of analogs. Additionally, we performed both *in vitro* MOA studies and *in vivo* PK assessments of the selected synthetic analogs.

Results and discussion

Structure–activity relationship study of the core structure of tirbanibulin

According to the co-crystal structure of **8** bound to colchicine (**9**)-binding site at the intradimer interface of α and β tubulins (PDB code: 6KNZ), the key ligand-protein interaction involves water-mediated hydrogen bonding. Both the nitrogen and oxygen atoms in the pyridinyl acetamide core act as hydrogen bonding acceptors, forming interactions with the adjacent Glu200 through a conserved water molecule.[25] Based on this and to understand the key SAR at the chemotype level, a series of tirbanibulin derivatives was initially synthesized by modification around the pyridinyl acetamide core (Scheme 1). Tirbanibulin (**8**) was prepared in gram scale, in two steps, from commercially available compound **10** (Scheme 1A). Amide coupling of **10** with benzylamine afforded compound **11**. Subsequent use of the cross-coupling Suzuki reaction with

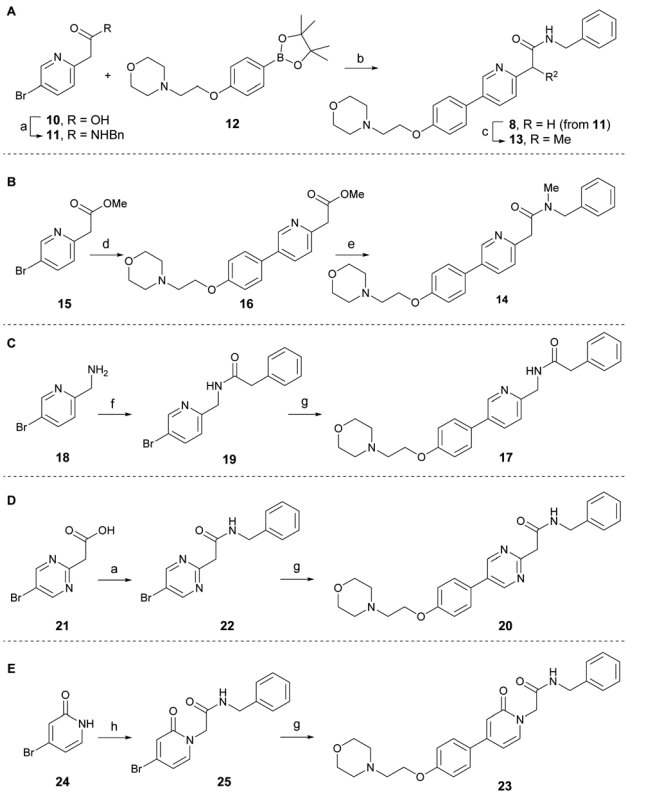

Scheme 1 Synthesis of tirbanibulin (**8**) and its derivatives. (a) benzylamine, EDC·HCl, HOBt, Et_3N, CH_2Cl_2, rt, 18 h and 77% for **11**; 6 h and 51% for **22**; (b) Pd(dppf)Cl_2·CH_2Cl_2, Cs_2CO_3, PPh_3, DMF/H_2O, 100 °C, 2 h, 80%. (c) MeI, NaH, DMF, rt, 30 min, 51%. (d) **12**, Pd(dppf)Cl_2·CH_2Cl_2, KF, PPh_3, DMF/H_2O, 100 °C, 4 h, 99%. (e) *N*-methyl benzylamine, TBD, 1,4-dioxane, 60 °C, 17 h, 63%. (f) phenylacetic acid, HATU, DIPEA, DMF, rt, 13 h, 62%. (g) **12**, Pd(dppf)Cl_2·CH_2Cl_2, Cs_2CO_3, PPh_3, DMF/H_2O, 100 °C, 2 h and 82% for **17**; 2 h and 36% for **20**; 20 h and 47% for **23**. (h) *N*-Benzyl-2-bromoacetamide, K_2CO_3, DMF, 100 °C, 3 h, 85%. EDC·HCl = *N*-(3-dimethylaminopropyl)-*N*′-ethylcarbodiimide hydrochloride, HATU = 1-[bis(dimethylamino)methylene]-1*H*-1,2,3-triazolo[4,5-*b*]pyridinium 3-oxid hexafluorophosphate, TBD = 1,5,7-triazabicyclo[4.4.0]dec-5-ene, DIPEA = *N*,*N*-diisopropylethylamine.

diboron **12** led to the synthesis of tirbanibulin (**8**). Further α-methylation by sodium hydride successfully yielded analog **13**, whereas selective *N*-methylation of **8** failed. Thus, *N*-methyl analog **14** was prepared from commercially available methyl ester **15** (Scheme 1B). The Suzuki reaction with **12** and subsequent aminolysis of the resulting compound **16**, by *N*-methyl benzylamine, efficiently provided analog **14**. The inverted amide analog **17** was prepared from amine **18** *via* coupling with phenylacetic acid and the Suzuki reaction of the resulting **19** with **12** (Scheme 1C). Pyrimidine analog **20** was synthesized using a similar procedure, starting from **21** and proceeding *via* **22** (Scheme 1D). For the synthesis of pyridone analog **23**, selective *N*-alkylation of bromopyridone **24** was performed to yield **25**, which underwent the Suzuki reaction with **12** (Scheme 1E).

The antitumor activity of the synthesized analogs was evaluated on HeLa cells using the CCK-8 assay (Table 1). Tirbanibulin (**8**) exhibited potent antiproliferative activity, with an IC_{50} value of 44 nM. However, the introduction of an α-methyl group to analog **13** significantly reduced its activity to submicromolar levels. This result suggests that the binding pocket surrounding the amide moiety of **8** in tubulins lacks the necessary space to accommodate even a small methyl group. The *N*-methylated analog **14** showed very weak antiproliferative activity. The inverted amide analog **17**, which possesses physicochemical properties highly similar to those of **8**, was less potent than **8**, indicating that a single hydrogen acceptor is probably not sufficient for optimal hydrogen bonding *via* water mediation. Retaining both the hydrogen acceptors, the pyridine core of **8** was replaced by alternative heteroaromatics, as exemplified by pyrimidine **20** and pyridone **23**. The potencies of **20** and **23** were greater than that of a series of amide-modified analogs (**13**, **14**, and **17**). Although potency of pyridone analog **23** was lower than that of tirbanibulin (**8**), compound **23** possessed a lower *c*Log*P* value. These results indicate that **23** could be employed in late-stage medicinal chemistry studies to improve solubility and metabolic stability.[28,29] Overall, these results demonstrate that both hydrogen acceptors in the central structure of **8** are required for optimal interaction with tubulins.

Synthesis and evaluation of amide-modified analogs

To develop new and potent microtubule inhibitors based on tirbanibulin (**8**), the bioactive conformation of **8** was considered. In the co-crystal structure (PDB code: 6KNZ),[25] **8** exists in a *cis*-amide conformation, which is energetically unfavorable. We hypothesized that the introduction of chemical modifications to mimic the *cis*-amide conformation would reduce the energy required for optimal ligand-protein binding, consequently enhancing the affinity and potency of the compound as a microtubule-targeting agent.

To incorporate the *cis*-amide bioisosteres in **8** while retaining the two hydrogen bonding acceptors, several analogs were designed and synthesized as shown in Scheme 2.[30] The representative bioisosteres for the *cis*-amide are 1,5-tetrazole or 1,5-triazole, both of which have been incorporated into various approved drugs.[30] The 1,5-tetrazole analog **26** was directly synthesized by the treatment of DPPA with inverted amide **17** (Scheme 2A).[31] The 1,5-triazole analog **27** in Scheme 2B was designed to have a hydroxy group at the benzylic position to induce additional interactions with adjacent Val238. An attempt to achieve the regioselective formation of 1,5-triazole from azide **28** (ref. 32) and α-ethynylbenzyl alcohol using ruthenium-catalyzed cycloaddition conditions yielded, only unidentified

Table 1 The antiproliferative activity of initial analogs against HeLa cells

Compound	HeLa IC_{50}[a,b] (μM)	*c*Log*P*[c]
8	0.044 ± 0.011	3.3
13	0.95 ± 0.35	3.7
14	>1.0	3.2
17	0.97 ± 0.23	3.3
20	0.37 ± 0.10	2.8
23	0.24 ± 0.06	2.6

[a] Data represent the mean of three independent determinations from triplicate samples. [b] IC_{50} values were determined using the CCK-8 assay in HeLa cells. [c] *c*Log*P* values were calculated using online ALOGPS 2.1 program.

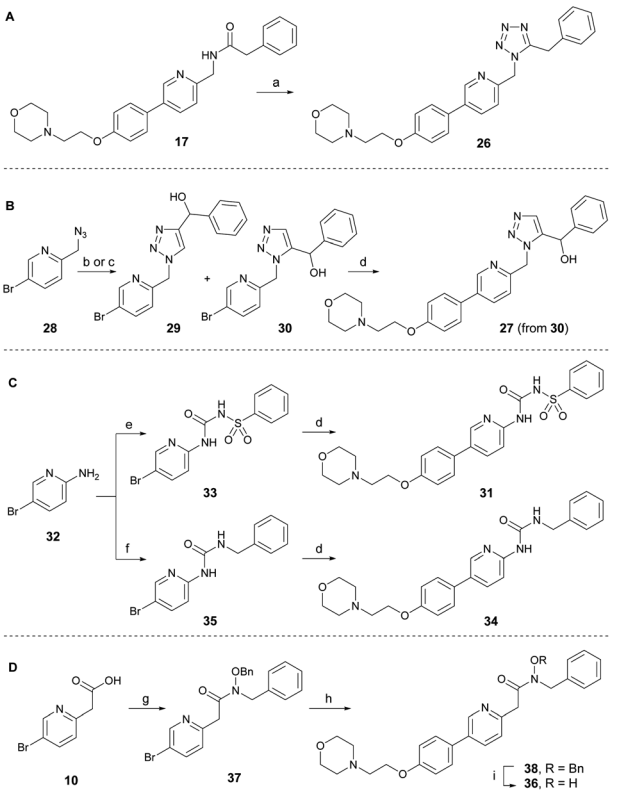

Scheme 2 Synthesis of amide-modified analogs. (a) DPPA, 4-picoline, 100 °C, 25 h, 68%. (b) phenylprop-2-yn-1-ol, toluene, 18 h, 68% (**29** and **30**). (c) $CuSO_4$, ascorbic acid, CH_3Cl/H_2O (3 : 1), rt, 14 h, 94% for **29**. (d) **12**, $Pd(dppf)Cl_2 \cdot CH_2Cl_2$, Cs_2CO_3, PPh_3, DMF/H_2O, 100 °C, 1 h and 79% for **27**; 40 min and 57% for **31**; 2 h and 37% for **34**. (e) benzenesulfonyl isocyanate, CH_2Cl_2, rt, 10 min, 76%; (f) benzyl isocyanate, THF, reflux, 6 h, 83%. (g) *N*,*O*-dibenzylhydroxylamine, EDC·HCl, HOBt, Et_3N, CH_2Cl_2, rt, 6 h, 78%; (h) **12**, $Pd(dppf)Cl_2 \cdot CH_2Cl_2$, KF, PPh_3, DMF/H_2O, 100 °C, 16 h, 22%. (i) Pd/C, H_2(g), MeOH, rt, 6 h, 84%. DPPA = diphenyl phosphoryl azide, EDC·HCl = *N*-(3-dimethylaminopropyl)-*N*′-ethylcarbodiimide hydrochloride.

Table 2 The antiproliferative activity of amide-modified tirbanibulin analogs against HeLa cells

Compound	HeLa IC_{50}[a,b] (μM)	*c*Log*P*[c]
8	0.044 ± 0.011	3.3
26	>4.0	2.9
27	>4.0	2.9
31	>4.0	2.9
34	0.78 ± 0.20	3.5
36	1.1 ± 0.4	3.4

[a] Data represent the mean of three independent determinations from triplicate samples. [b] IC_{50} values were determined using the CCK-8 assay in HeLa cells. [c] *c*Log*P* values were calculated using online ALOGPS 2.1 program.

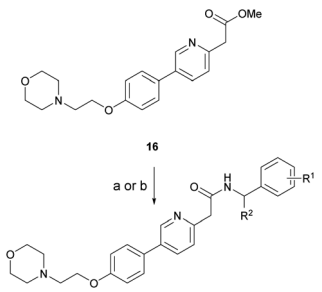

Scheme 3 Synthesis of benzylamine-modified analogs *via* ester aminolysis. (a) amines, DBU, 1,4-dioxane, microwave, 180–200 °C, 2 h. (b) amines, TBD, 1,4-dioxane, 60 °C, 15 h–4 d. DBU = 1,8-diazabicyclo [5.4.0]undec-7-ene, TBD = 1,5,7-triazabicyclo[4.4.0]dec-5-ene.

side products and no detectable desired product.[33] As an alternative approach, thermal azide–alkyne cycloaddition reactions were conducted in the absence of catalyst, leading to a separable mixture of regioisomers (**29** : **30** = 1 : 1) with a combined yield of 68%. The desired intermediate **30** was subsequently transformed into triazole analog **27** *via* the Suzuki reaction. The structure of **30** was indirectly confirmed by exclusively obtaining the 1,4-regioisomer **29** through a regiospecific Cu(I)-catalyzed 1,3-dipolar cycloaddition of **28** with α-ethynylbenzyl alcohol.[34] To enhance the molecular conformational rigidity, a sulfonyl urea analog **31** was designed to possess intramolecular hydrogen bonding, which aimed to mimic the *cis*-amide conformation; with lower N–H proton acidity for improved hydrogen bonding interactions (Scheme 2C). Aminopyridine **32** reacted with benzenesulfonyl isocyanate to produce **33**, which upon Suzuki reaction was converted to analog **31**. Urea analog **34** was synthesized from **32** through the intermediate **35**. The *N*-hydroxy amide **36** was also designed to possess intramolecular hydrogen bonding. It was prepared from acid **10** through several synthetic steps: amide coupling with hydroxylamine, a Suzuki reaction with the resulting amide **37**, and a subsequent debenzylation of **38** (Scheme 2D). The *cis*-amide bioisostere analogs, 1,5-tetrazole **26** and 1,5-triazole **27**, exhibited no antitumor activity, even at the maximum concentration of 4.0 μM (Table 2). Sulfonylurea **31**, designed to induce rigidity through intramolecular hydrogen bonding, was ineffective against cancer cells, partly owing to the planarity of the urea moiety, as is evident from the reduced potency of the urea analog **34**. *N*-hydroxy amide analog **36** displayed only modest antiproliferative activity at a micromolar level. Consequently, amide modification using other isosteres did not offer sufficient potency to justify further investigation.

Synthesis and evaluation of benzylamine-modified analogs

Based on the SAR study, our efforts shifted towards modifying the benzylamine moiety while preserving the core amide structure, connected with either pyridine or pyridone. Co-crystal structural analysis revealed a limited binding site around the benzylamine moiety of **8**, making it unsuitable for large substituents. The binding site consisted of several polar amino acid residues (Tyr52, Gln136, and Asn167). Therefore, the design of analogs ruled out the use of large substituents and prioritized small or polar substituents as well as heteroaromatics. As shown in Scheme 3, the aminolysis of **16** with diverse amines afforded the designed benzylamine-modified analogs.

Heteroaromatic analogs **39** and **40**, including pyridine and pyrimidine, respectively, exhibited weak cellular activity only at a micromolar level (Table 3). Phenol **41** was designed for the additional hydrogen bonding interaction between the hydroxy group of **41** and Glu200 in the binding pocket. However, a micromolar IC_{50} value was observed. The *ortho*- and *meta*-methylated **42** and **43** were ineffective. However, *para*-methylated **44** was equipotent to tirbanibulin (**8**) (**44**: IC_{50} = 27 nM *vs.* **8**: IC_{50} = 44 nM), indicating that the *para*-substituent was tolerable. A similar trend was observed in a series of fluorinated analogs (**45–47**), where *para*-fluorinated **47** showed a potency comparable to **8** with an IC_{50} value of 40 nM. Analog **48** with a *para*-CF_3 group, with a stronger electron-withdrawing effect than fluoride, was 7-fold less potent than compound **47**, despite having a higher *c*Log*P* value which potentially indicates high cell permeability. The potency of *para*-methoxy analog **49** was reduced to micromolar levels, whereas methylamino analog **50** exhibited significant activity with an IC_{50} value of 0.15 μM. Compound **50** was the most potent in a series of related analogs such as aniline **51** and *N,N*-dimethyl analog **52**. Saturation of the benzyl moiety (analog **53**) had a negative impact on potency, indicating the importance of the π-interaction of the benzene ring with surrounding amino acid residues. Furthermore, the addition of a small methyl group at the amino-benzylic position of **8**, which would be beneficial for hydrophobic interactions with the surrounding residues, was evaluated. We presumed that the addition of (*S*)-methyl group would be more efficient than (*R*)-methyl group since the pro-(*R*) hydrogen already interacts with the backbone carbonyl oxygen of Val238 in the co-crystal structure. As expected, (*S*)–Me compound **54** was more potent than the (*R*)–Me compound **55** (**54**: IC_{50} = 0.45 μM *vs.* **55**: IC_{50} > 4.0 μM), although the growth inhibition activity of **54** was still insufficient. In addition, *para*-methyl and fluorine substituents that elicited potency equal to that of tirbanibulin were incorporated into pyridone analogs **56** and **57**. The methylated analog **56** showed the potency improvement compared to the pyridone analog **23** (**56**: IC_{50} = 0.25 μM *vs.* **23**: IC_{50} = 0.24 μM), while the cellular potency was similar for the fluorinated compound **57**.

Table 3 The antiproliferative activity of benzylamine-modified tirbanibulin analogs against HeLa cells

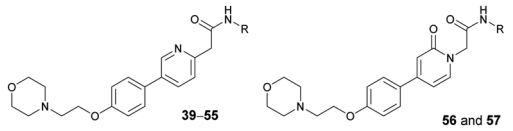

Compound	R	HeLa IC_{50}[a,b] (μM)	cLogP[c]	Compound	R	HeLa IC_{50}[a,b] (μM)	cLogP[c]
8		0.044 ± 0.011	3.3	**48**	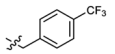	0.27 ± 0.07	4.0
39		>4.0	2.8	**49**	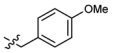	2.0 ± 0.5	3.2
40		>4.0	2.8	**50**	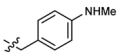	0.15 ± 0.04	2.7
41		2.1 ± 0.6	3.0	**51**	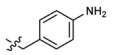	0.63 ± 0.07	2.0
42		2.2 ± 0.5	3.5	**52**	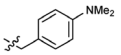	0.48 ± 0.06	3.4
43	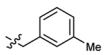	0.97 ± 0.22	3.5	**53**		>4.0	4.2
44	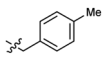	0.027 ± 0.004	3.5	**54**		0.45 ± 0.10	3.6
45		0.26 ± 0.06	3.4	**55**		>4.0	3.6
46		0.53 ± 0.15	3.4	**56**	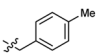	0.25 ± 0.06	3.6
47		0.040 ± 0.009	3.4	**57**		0.34 ± 0.11	3.3

[a] Data represent the mean of three independent determinations from triplicate samples. [b] IC_{50} values were determined using the CCK-8 assay in HeLa cells. [c] *cLogP* values were calculated using online ALOGPS 2.1 program.

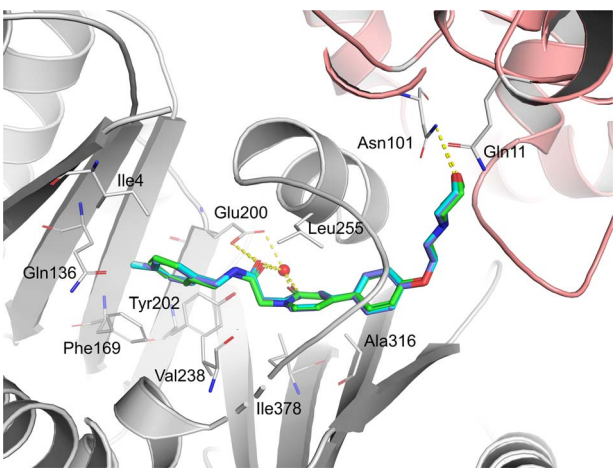

Fig. 1 Predicted and superimposed binding poses of pyridone analog **23** (green), *p*-Me analog **44** (cyan) and *p*-F analog **47** (blue) in the colchicine-binding site of tubulin (A-chain: salmon, B-chain: gray).

Molecular docking simulation

To further investigate the binding modes of the selected compounds, a molecular modeling study was performed. The ligand binding modes of compounds **44** and **47** were almost identical to those of tirbanibulin (Fig. 1). The main binding affinities were water-mediated hydrogen bonds and direct interactions with the B-chain of tubulin. Specifically, the amide carbonyl group and nitrogen atom in pyridine, both of which reside in compounds **44** and **47**, participate in water-mediated hydrogen bonding with Glu200, whereas the amide carbonyl group forms an additional direct hydrogen bond with Glu200. Notably, the addition of *para*-substituents to the benzene moiety did not change the binding mode. Instead, methyl and fluorine groups were positioned in the hydrophobic pocket formed by Ile4, Gln136, Phe169, and Tyr202, implying that these substituents could be further utilized to design a molecule with improved affinity with tubulins. Additionally, the replacement of pyridine in **8** with pyridone in **23** showed an almost identical binding mode, according to this docking model.

Table 4 Mouse pharmacokinetic parameters of compounds **44** and **47**

	i.v.[a] (2 mg kg^{-1})				p.o.[b] (10 mg kg^{-1})			
Compound	AUC_{last} (μg h mL^{-1})	$t_{1/2}$ (h)	CL (L h^{-1} kg^{-1})	*V*ss (L kg^{-1})	AUC_{last} (μg h mL^{-1})	C_{max} (μg mL^{-1})	$t_{1/2}$ (h)	*F* %
44	0.77 ± 0.04	7.05 ± 1.92	2.58 ± 0.15	1.89 ± 0.31	0.94 ± 0.16	1.54 ± 0.33	5.45 ± 1.48	24
47	0.84 ± 0.11	1.69 ± 1.09	2.39 ± 0.32	3.23 ± 0.81	4.88 ± 2.07	2.88 ± 1.22	2.30 ± 0.23	116

[a] Dosed at 2 mg kg^{-1} for i. v. administration of ICR mouse ($n = 3$, mean ± SD) in 5% DMSO/40% PEG400/55% DW (5 mL kg^{-1}). [b] Dosed at 10 mg kg^{-1} for p. o. administration of ICR mouse ($n = 3$, mean ± SD) in 5% DMSO/40% PEG400/55% DW (5 mL kg^{-1}).

Table 5 *In vitro* microsomal stability and plasma protein binding of representative analogs

	Microsomal stability (%)[a]		Plasma protein binding rate (%)	
Compound	Mouse	Human	Mouse	Human
8	67.7 ± 5.6	50.7 ± 3.2	84.8 ± 3.4	81.3 ± 2.0
44	15.7 ± 0.4	1.4 ± 0.1	94.3 ± 0.6	93.5 ± 0.6
47	38.6 ± 0.6	21.8 ± 1.4	89.3 ± 1.0	87.4 ± 2.4
56	50.6 ± 1.2	20.2 ± 2.3	96.0 ± 0.2	82.9 ± 0.5

[a] Percentage of test compounds remaining after 30 min in mouse and human liver microsomes in the presence of NADPH (phase I stability).

In vitro ADME and *in vivo* PK

As equipotent molecules to **8**, compounds **44**, **47**, and **56** were further evaluated by *in vitro* ADME, including microsomal stability and plasma protein binding. Tirbanibulin (**8**) showed good microsomal stability in both mice and humans, with over 50% remaining at 30 min. The *para*-methylated analog **44** was found to be very unstable in liver microsomes, likely because of oxidative liability at the benzylic position of the toluene moiety. Exchange of Me with F, as shown in compound **47**, resulted in improved microsomal stability. Furthermore, the metabolic stability of the *para*-methylbenzene moiety in **44** was improved by changing the pyridine core to pyridone in **56**, likely due to a decrease in lipophilicity. The percentage of plasma protein binding of all compounds was within acceptable ranges.

Further evaluation of the *para*-substituted compounds **44** and **47** was conducted using animal PK studies. Both compounds exhibited moderate clearance (Table 5). Compound **44**, however, showed an oral bioavailability of less than 25%, resulting in a low oral AUC and C_{max}. This was likely due to the first-pass effect, which is supported by the microsomal instability of compound **44** (Table 4). In contrast, a high oral AUC value of the fluorinated **47** was observed at 4.0 μg h mL^{-1}; 4-fold higher than that of compound **44**, despite a shorter half-life (Table 5). In addition, compound **47** showed an excellent oral bioavailability ($F = 116\%$). These findings suggest that fluorine can be effectively utilized for further chemical modification of the benzylamine moiety of **8**, considering its effects on potency and PK profiles.

Confirmation of mechanism of action and biocompatibility

Next, we aimed to confirm the MOA of the representative analog **47** using several *in vitro* assays. We performed a cell cycle assay

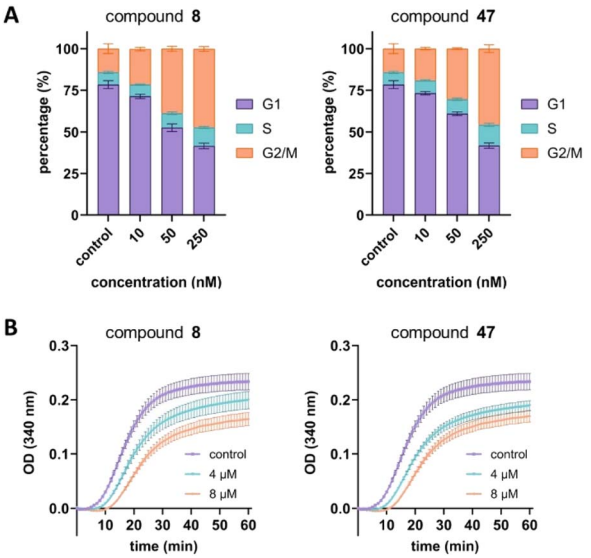

Fig. 2 Confirmation of mechanism of action. (A) Cell cycle assay conducted in HeLa cells for compound **8** and **47**. The *p* values of G2/M percentages for both compounds **8** and **47** are <0.0001 (one-way ANOVA). (B) Tubulin polymerization assay of compound **8** and **47**. The *p* values for both compounds **8** and **47** are <0.0001 (two-way ANOVA).

using HeLa cells to analyze the proportion of the cell population in each phase. Similar to tirbanibulin (**8**), analog **47** induced G2/M phase arrest in a concentration-dependent manner, which is a key MTA characteristic (Fig. 2A). The results of the tubulin polymerization assay indicated that, like tirbanibulin (**8**), analog **47** is microtubule destabilizers; with greater depolymerization observed with increasing chemical concentration from 0 to 8 μM (Fig. 2B). These findings suggest that *para*-fluorinated **47** targets microtubules and causes an antiproliferative effect by disrupting tubulin polymerization.

Src inhibition is an additional MOA of tirbanibulin.[18–20] Tirbanibulin disrupts the Src signaling pathway by binding to the peptide substrate-binding site, which is distinct from conventional ATP-competitive kinase inhibitors. Considering that Src is strongly associated with various malignancies,[35,36] it would be beneficial if the designed analog could retain its Src inhibitory capability. We investigated the inhibition of target protein phosphorylation in HeLa cells exposed to compound **47**. When compound **47** was treated to the HeLa cells, a reduction in p-Src and p-FAK levels was observed even at a low concentration (50 nM), while total Src and FAK levels remained unchanged (Fig. 3A). Notably, compound **47** demonstrated an enhanced

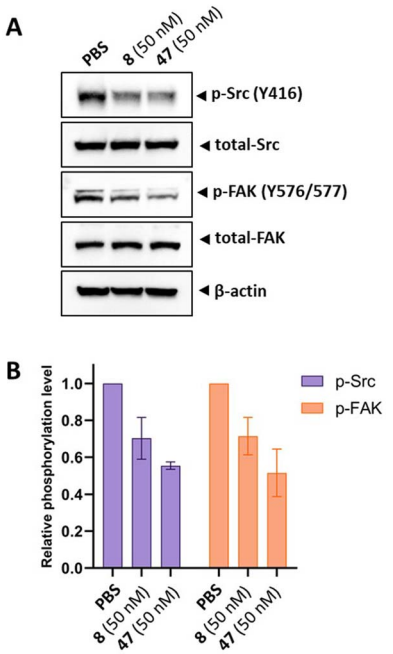

Fig. 3 Western blot analysis of p-Src and p-FAK in the protein samples obtained from HeLa cells treated with PBS, **8** (50 nM), and **47** (50 nM) for 6 h. (A) Western blot image. (B) Relative phosphorylation level of Src and FAK.

inhibitory ability for the phosphorylation of Src and FAK compared to compound **8** (Fig. 3B). This suggests that *para* fluorination on the benzylamine moiety could improve the inhibitory effect on Src by preserving the molecule's binding to the peptide substrate site of Src.

Additionally, compound **47**'s biocompatibility was evaluated through *in vitro* cytotoxicity assays using three normal cell lines (MCF-10A, CCD-18Co, and BJ). Treatment with concentrations below 4 μM for compound **47** demonstrated no significant cytotoxic effects on these non-tumorigenic cells, and their cell morphologies remained mostly unaltered (Fig. S5 in the ESI†).[37,38] This outcome suggests the safety of compound **47**, considering its double-digit nanomolar IC_{50} value (**47**'s IC_{50} = 40 nM) against HeLa cancer cells.

Conclusions

In summary, we designed and synthesized a series of tirbanibulin-based analogs, including the amide- and benzylamine-modified versions. Initial SAR study, conducted for the efficient design of derivatives, highlighted the importance of the core pyridinyl acetamide structure with two hydrogen bonding acceptors. Amide-modified analogs designed to mimic the bioactive *cis*-amide conformation were ineffective in terms of cytotoxicity. In contrast, *para* substitution of the benzylamine moiety provided several equipotent derivatives, represented by *para*-fluorinated **47**. This analog also displayed favorable *in vivo* PK properties, with an excellent oral bioavailability. The mechanism of action was identified to involve both the microtubule-destabilizing effect and Src inhibition. Notably, the Src inhibitory effect of compound **47** was observed to be improved compared to that of tirbanibulin, showing another advantage of *para* fluorination of the benzylamine part of tirbanibulin. Overall, these results provide guidance for future optimization and development of new tirbanibulin-based molecules as anticancer agents. While this study focused on the structural variation of tirbanibulin in the amide motif and C-ring, the results from our medicinal chemistry program, which encompasses the systemic variation of tirbanibulin, including derivatization of A/B-ring, will be reported in due course.

Experimental

General information

The most reagents used in this study were purchased from Sigma-Aldrich (St. Louis, MO, USA), TCI (Tokyo, Japan), Alfa Aesar (Auburn Hills, MI, USA), BLDpharm (Telangana, India), and so forth, and used without further purification. The progress of the reaction was confirmed by thin layer chromatography (TLC) using TLC silica gel 60 F254, 0.25 mm (Merck, St, Louis, MO, USA). Separation processes were carried out using either medium-pressure liquid chromatography (CombiFlash NEXTGEN 300+ [Teledyne ISCO, Lincoln, NE, USA]) using a column cartridge (4–120 g, RediSep®Rf) or high-performance liquid chromatography (HPLC) (YL9100 Semi-prep HPLC system with YL9101S Vacuum Degasser, YL9111S Binary Pump, and YL9120S UV/Vis Detector) and Agilent 5 Prep-C18 × 21.2 mm column cartridge. Mass spectroscopy of the products was identified by Agilent 6130 Quadrupole liquid chromatography-mass spectrometer (LC/MS). High-resolution mass spectrometry of the compounds was obtained using either the FAB or EI mode, with a resolution of 10 000, employing the JEOL JMS-700 High-Resolution Mass Spectrometer (HRMS). Nuclear magnetic resonance (NMR) spectra for the structural analysis of the products were measured by Bruker UltraShield 300 MHz, 400 MHz, and 500 MHz NMR spectrometers. Most of NMR solvents were purchased from Cambridge Isotope Laboratories such as chloroform-*d*, methanol-d_4, and dimethylsulfoxide-d_6.

Cell viability assay

Cells were purchased from ATCC (Manassas, VA). Cells were cultured in RPMI-1640 medium (Gibco, Thermo Fisher Scientific, Waltham, MA) supplemented with 10% fetal bovine serum (Gibco) and 1% penicillin-streptomycin (Gibco) at 37 °C and 5% CO_2. One day prior to drug treatment, 10 000 cells of each cell line were seeded into 96-well plates in 100 μL of RPMI-1640 medium. On the following day, the cells were treated with test compounds solubilized in dimethyl sulfoxide (Sigma-Aldrich, St. Louis, MO). After 48 h of drug treatment, 10 μL of CCK-8 reagent was added to each well, and the absorbance at 450 nm was measured using a SpectraMax iD5 spectrophotometer (Molecular Devices, San Jose, CA). The absorbance signal at 450 nm is proportional to the number of viable cells.

Cell cycle assay

To study the effects of test compounds on the cell cycle, a Muse cell cycle kit (Luminex, Austin, TX) was used. The experimental protocol followed the manufacturer's instructions. First, 1×10^6 cells were grown in 6-well cell culture plates (Corning, Corning, NY). The cells were then treated with compounds for 48 hours. After treatment, the cells were collected and fixed with 70% pure ethanol. The fixed cells were then frozen at −20 °C for 12 h and stained with a cell cycle reagent for 30 min at room temperature in the dark. Finally, the fixed and stained cells were analyzed with a Muse cell analyzer (Luminex).

Tubulin polymerization assay

A tubulin polymerization assay kit (Cytoskeleton Inc., Denver, CO) was used to evaluate the activity of test compounds. The assay protocol strictly followed the manufacturer's instructions. In brief, test compounds were mixed with tubulin in the general tubulin buffer provided by the manufacturer. Tubulin polymerization reactions were then monitored for 1 h at 37 °C in a SpectraMax iD5 spectrophotometer (Molecular Devices, San Jose, CA) with an absorbance wavelength of 340 nanometers.

Western blot assay

To investigate the effect of the compound on the target signaling pathway, western blot assay was conducted. HeLa cells were treated either with compounds (50 nM) or PBS (control group) for 6 hours and then, proteins were extracted. Equal amounts of proteins were resolved SDS-polyacrylamide gel electrophoresis (SDS-PAGE) and transferred to polyvinylidene difluoride (PVDF) membranes. After blocking with buffer, the blot was incubated with primary antibodies, and then incubated with the appropriate secondary antibodies.

Molecular modelling

The Maestro software in the Schrodinger Suite was utilized in the molecular modelling studies.[39] The crystal structure of tubulins was obtained from the Protein Data Bank (PDB code: 6KNZ), and any structural defects were rectified using the Protein Preparation Workflow module. The structures of selected compounds were docked against the colchicine binding site using the Glide docking module, following standard protocols. The reproduction of crystal ligand poses with a good root mean square displacement of 0.3 Å demonstrated the robustness of our docking protocol. The best-docked pose, characterized by the lowest Glide score, was selected for the subsequent binding pose analysis.

Statistical analysis

Statistical analysis was performed using GraphPad Prism 10 software (GraphPad Software, San Diego, CA, USA) and Origin 8.5 (OriginLab Corporation, Northampton, MA, USA). The values are expressed as the mean ± standard error of means. The significance between means was tested using one-way or two-way ANOVA. The Dunnett test was conducted to compare every mean to a control mean. A value of $P < 0.05$ was considered significant.

Author contributions

HJ conceived the study, wrote the manuscript, and obtained the necessary funding. JP, MK, and AL were responsible for compound synthesis, purification, and characterization. BK conducted the *in vitro* assays, including the cell viability assay, cell cycle assay, and tubulin polymerization assay. KC performed the western blotting assay. CC was responsible for computational modeling and docking studies.

Conflicts of interest

There are no conflicts to declare.

Acknowledgements

This work was supported by the National Research Foundation of Korea (NRF) grant funded by the Korean government (MSIT) (2022R1C1C1004145). It also received support from Korea Research Institute of Chemical Technology (KK2331-20).

Notes and references

1 A. Serrano-del Valle, C. Reina-Ortiz, A. Benedi, A. Anel, J. Naval and I. Marzo, *Biochem. Pharmacol.*, 2021, **190**, 114655.
2 J. Tischer and F. Gergely, *J. Cell Biol.*, 2018, **218**, 10–11.
3 M. Haschka, G. Karbon, L. L. Fava and A. Villunger, *EMBO Rep.*, 2018, **19**, e45440.
4 C. Dominguez-Brauer, K. L. Thu, J. M. Mason, H. Blaser, M. R. Bray and T. W. Mak, *Mol. Cell*, 2015, **60**, 524–536.
5 K. S. Chan, C. G. Koh and H. Y. Li, *Cell Death Dis.*, 2012, **3**, e411.
6 L. Wordeman and J. J. Vicente, *Cancers*, 2021, **13**, 5650.
7 V. Čermák, V. Dostál, M. Jelínek, L. Libusová, J. Kovář, D. Rösel and J. Brábek, *Eur. J. Cell Biol.*, 2020, **99**, 151075.
8 M. O. Steinmetz and A. E. Prota, *Trends Cell Biol.*, 2018, **28**, 776–792.
9 E. Mukhtar, V. M. Adhami and H. Mukhtar, *Mol. Cancer Ther.*, 2014, **13**, 275–284.
10 A. C. Borisa and H. G. Bhatt, *Eur. J. Med. Chem.*, 2017, **140**, 1–19.
11 X. Liu, *Transl. Oncol.*, 2015, **8**, 185–195.
12 I. Garcia-Saez and D. A. Skoufias, *Biochem. Pharmacol.*, 2021, **184**, 114364.
13 A. A. El-Arabey, S. A. Salama and A. R. Abd-Allah, *Life Sci.*, 2018, **208**, 192–200.
14 A. L. Parker, M. Kavallaris and J. A. McCarroll, *Front. Oncol.*, 2014, **4**, 153–172.
15 C. Dumontet, J. M. Reichert, P. D. Senter, J. M. Lambert and A. Beck, *Nat. Rev. Drug Discovery*, 2023, **22**, 641–661.
16 W. Shuai, G. Wang, Y. Zhang, F. Bu, S. Zhang, D. D. Miller, W. Li, L. Ouyang and Y. Wang, *J. Med. Chem.*, 2021, **64**, 7963–7990.
17 K. E. Arnst, S. Banerjee, H. Chen, S. Deng, D.-J. Hwang, W. Li and D. D. Miller, *Med. Res. Rev.*, 2019, **39**, 1398–1426.

18 Y. Gilaberte and M. T. Fernández-Figueras, *Actas Dermo-Sifiliogr.*, 2022, **113**, T58–T66.
19 S. Kim, A. Min, K.-H. Lee, Y. Yang, T.-Y. Kim, J. M. Lim, S. J. Park, H.-J. Nam, J. E. Kim, S.-H. Song, S.-W. Han, D.-Y. Oh, J. H. Kim, T.-Y. Kim, D. Hangauer, J. Y.-N. Lau, K. Im, D. S. Lee, Y.-J. Bang and S.-A. Im, *Cancer Res. Treat.*, 2017, **49**, 643–655.
20 M. P. Smolinski, Y. Bu, J. Clements, I. H. Gelman, T. Hegab, D. L. Cutler, J. W. S. Fang, G. Fetterly, R. Kwan, A. Barnett, J. Y. N. Lau and D. G. Hangauer, *J. Med. Chem.*, 2018, **61**, 4704–4719.
21 E. S. Antonarakis, E. I. Heath, E. M. Posadas, E. Y. Yu, M. R. Harrison, J. Y. Bruce, S. Y. Cho, G. E. Wilding, G. J. Fetterly, D. G. Hangauer, M.-F. R. Kwan, L. M. Dyster and M. A. Carducci, *Cancer Chemother. Pharmacol.*, 2013, **71**, 883–892.
22 A. Blauvelt, S. Kempers, E. Lain, T. Schlesinger, S. Tyring, S. Forman, G. Ablon, G. Martin, H. Wang, D. L. Cutler, J. Fang and M.-F. R. Kwan, *N. Engl. J. Med.*, 2021, **384**, 512–520.
23 A. Moore, K. Hurley and S. A. Moore, *JAAD Case Rep*, 2022, **28**, 11–13.
24 J.-B. Hong, P.-Y. Wu, A. Qin, Y.-W. Huang, K.-C. Tseng, C.-Y. Lai, W.-K. Chan, J. Fang, D. L. Cutler and T.-F. Tsai, *Pharmaceutics*, 2022, **14**, 2159.
25 L. Niu, J. Yang, W. Yan, Y. Yu, Y. Zheng, H. Ye, Q. Chen and L. Chen, *J. Biol. Chem.*, 2019, **294**, 18099–18108.
26 A. Fallah-Tafti, A. Foroumadi, R. Tiwari, A. N. Shirazi, D. G. Hangauer, Y. Bu, T. Akbarzadeh, K. Parang and A. Shafiee, *Eur. J. Med. Chem.*, 2011, **46**, 4853–4858.
27 L. Wang, Y. Zheng, D. Li, J. Yang, L. Lei, W. Yan, W. Zheng, M. Tang, M. Shi, R. Zhang, X. Cai, H. Ni, X. Ma, N. Li, F. Hong, H. Ye and L. Chen, *J. Med. Chem.*, 2021, **64**, 8127–8141.
28 Y. Zhang and A. Pike, *Bioorg. Med. Chem. Lett.*, 2021, **38**, 127849.
29 D. F. V. Lewis and M. Dickins, *Drug Metab. Rev.*, 2003, **35**, 1–18.
30 S. Kumari, A. V. Carmona, A. K. Tiwari and P. C. Trippier, *J. Med. Chem.*, 2020, **63**, 12290–12358.
31 K. Ishihara, T. Shioiri and M. Matsugi, *Org. Lett.*, 2020, **22**, 6244–6247.
32 B. Guo, H. Fan, Q. Xin, W. Chu, H. Wang, Y. Huang, X. Chen and Y. Yang, *J. Med. Chem.*, 2013, **56**, 2642–2650.
33 J. R. Johansson, T. Beke-Somfai, A. Said Stålsmeden and N. Kann, *Chem. Rev.*, 2016, **116**, 14726–14768.
34 V. V. Rostovtsev, L. G. Green, V. V. Fokin and K. B. Sharpless, *Angew. Chem., Int. Ed.*, 2002, **41**, 2596–2599.
35 S. Martellucci, L. Clementi, S. Sabetta, V. Mattei, L. Botta and A. Angelucci, *Cancers*, 2020, **12**, 1448.
36 S. G. Pelaz and A. Tabernero, *Oncogene*, 2022, **41**, 4917–4928.
37 M. Anbalagan, A. Ali, R. K. Jones, C. G. Marsden, M. Sheng, L. Carrier, Y. Bu, D. Hangauer and B. G. Rowan, *Mol. Cancer Ther.*, 2012, **11**, 1936–1947.
38 M. Anbalagan, L. Carrier, S. Glodowski, D. Hangauer, B. Shan and B. G. Rowan, *Breast Cancer Res. Treat.*, 2012, **132**, 391–409.
39 *Schrödinger Release 2023-3: Maestro*, Schrödinger, LLC, New York, NY, 2023.